processes

MDPI

Article

Research on Flexible Braking Control of a Crawler Crane during the Free-Fall Hook Process

Wei Gao [1], Shiheng Song [1], Guisheng Yang [2], Chunyi Wang [3], Yong Wang [2], Lijuan Chen [1], Wenqiang Xu [2] and Chao Ai [2,*]

[1] School of Mechanical Engineering, Nanjing Institute of Technology, Nanjing 211167, China; gaowei2018@njit.edu.cn (W.G.); y00450210128@njit.edu.cn (S.S.); chenlj@njit.edu.cn (L.C.)
[2] School of Mechanical Engineering, Yanshan University, Qinhuangdao 066004, China; yanggs@stumail.ysu.edu.cn (G.Y.); wangyong123@stumail.ysu.edu.cn (Y.W.); 1526922762@stumail.ysu.edu.cn (W.X.)
[3] Zhejiang Sany Equipment Company Limited, Huzhou 200120, China; wangcy29@sany.com.cn
* Correspondence: aichao@ysu.edu.cn

Abstract: Due to the large inertia and strong impact accompanying the free-falling hook process of crawler cranes, it is difficult to meet the demand for flexible and smooth braking control under different weight load conditions. Therefore, this paper takes the free-fall hook system as the research object and combines system operation characteristics and control theory to carry out research on flexible braking control of the free-fall hook system. Firstly, a joint simulation platform of MATLAB (version 2018b) and AMESim (version 2019.1) software is built to theoretically analyze the key components of the free-fall hook system (proportional pressure-reducing valve, winch reducer, and wet clutch). Secondly, a mathematical model of the braking process is established, and the pressure control demand is clarified to analyze the reasons for the existence of dead zones and hysteresis loops in the system. Meanwhile, it is found that the dead zones and hysteresis loops existing in the pressure output of the pressure-reducing valve are the main factors of flexibility with load braking. Then, in this paper, a closed-loop control strategy is formulated based on the automatic adaptation of the braking gear in combination with the fuzzy PID pressure. Finally, the effectiveness of the control strategy proposed in this paper is verified with simulation and experimental testing using the pressure hysteresis loop of the free-fall hook process and the load-braking acceleration as the judging criteria. The results show that the system pressure hysteresis loop is reduced by 50%–60% and the maximum braking acceleration is reduced by 24%–30% under the conditions of 6.44 tonnes and 10.44 tonnes, which improves the accuracy of pressure control and achieves flexible and smooth braking with loads for different tonnages of free-fall hooks.

Keywords: free-fall hook; proportional pressure-reducing valve; wet clutch; pressure control; smooth braking

check for updates

Citation: Gao, W.; Song, S.; Yang, G.; Wang, C.; Wang, Y.; Chen, L.; Xu, W.; Ai, C. Research on Flexible Braking Control of a Crawler Crane during the Free-Fall Hook Process. *Processes* **2024**, *12*, 250. https://doi.org/10.3390/pr12020250

Academic Editor: Olympia Roeva

Received: 22 December 2023
Revised: 18 January 2024
Accepted: 20 January 2024
Published: 24 January 2024

Copyright: © 2024 by the authors. Licensee MDPI, Basel, Switzerland. This article is an open access article distributed under the terms and conditions of the Creative Commons Attribution (CC BY) license (https://creativecommons.org/licenses/by/4.0/).

1. Introduction

The free-fall hook system is an important part of a crawler crane, and the free-fall hook condition is one of the necessary capabilities of crawler cranes. However, due to the large inertia of the load during braking in the free-fall hook condition, as well as the influence of nonlinear factors and coupling characteristics, shocks and vibrations are easily caused. When shock and vibration phenomena are serious, a vehicle is at risk of tipping over [1–3].

The effect of a free-fall hook with load braking flexibility depends mainly on the stability and accuracy of the torque output of the wet multi-disc clutch, which depends on the pressure in the clutch control chamber and the friction characteristics of the clutch itself [4,5].

Wang and Wu et al. [6,7] studied the friction coefficient of the friction vice surface temperature, relative speed, roughness, contact load, and other factors of the common

effect of the friction coefficient. Zhang et al. [8] investigated the phenomenon of friction torque attenuation in the sliding film process of a wet multi-disc clutch, and they found that the torque decay coefficient is affected by relative speed and the average surface pressure. Yang et al. [9] determined that clutch engagement pressure affects the engagement time and that the torque jitter at the moment of contact depends on the stability of the engagement pressure. Meng et al. [10] revealed the contact characteristics of a clutch friction pair at the initial stage of braking. Liu et al. [11–14] investigated the effect of material parameters on the contact pressure distribution of clutches and proposed using the Pressure Distribution Index (PDI) to evaluate the pressure difference between a friction pair. Bao et al. [15] analyzed the working principle and motion process of a wet clutch and established a dynamic engagement model of the spring, piston, friction pair, and pressure plate. They found that improving the quality of the friction plate would reduce the engagement time.

Scholars at home and abroad have performed a lot of research on the pressure control of the clutch control chamber. Lu et al. [16] proposed a global terminal control algorithm based on the expansion state observer by tracking the deviation occurring in the clutch oil pressure control process in real time, thus improving the suppleness of the clutch binding process. Kuang [17] proposed a clutch pressure control algorithm based on a nonlinear feed-forward controller to accurately achieve clutch pressure in accordance with the target trajectory. Fu et al. [18] proposed a model-free adaptive predictive control (MFAPC) algorithm for clutch pressure based on the dynamic linearization of the tight format. Their results proved that the proposed algorithm has a better control tracking effect and robustness than algorithms such as PID, MFAC, etc., and the system has a better dynamic performance, which is conducive to improving the quality of power shift. Zhang et al. [19] used a motor-controlled pump to achieve pressure control and proposed a model-based nonlinear three-step controller to control the internal pressure of the actuator. Their results showed that the oscillation of the pressure control process is significantly reduced, the pressure response is faster, and the pressure control is more accurate. Qin et al. [20] proposed a joint pressure control method with a variable speed hydraulic pump and an electroproportional relief valve, and the results showed that this control strategy can expand the pressure control range and has better robustness than PID and slip film control to improve the pressure control accuracy. Zhang et al. [21,22] constructed a pressure controller for wet clutches based on the model-free adaptive control (PFDL-MFAC) algorithm with biased format dynamic linearization, which has better response speed and robustness compared with PID, and at the same time, improves the quality of clutch adhesion.

The above research on the friction characteristics of the clutch and pressure control provides a certain direction for the research in this paper. These control strategies yield favorable results within their respective systems, contingent upon accurate system modeling or reasonable parameter adaptive laws. These studies generally occur under specific environmental conditions, often ignoring the effects of nonlinear factors on the system. However, the free-fall hook system needs to have the ability to complete fast and flexible braking under large inertia load conditions, and it is necessary to take into account the characteristics of the free-fall hook working conditions as well as the characteristics of the system. Therefore, this paper uses the free-fall hook system proportional pressure-reducing valve, clutch, and other key components of the model to clarify if the nonlinear characteristics of the free-fall hook system, combined with the fuzzy PID control method that does not depend on the model accuracy, are suitable for solving the nonlinear, strong coupling time-varying, hysteresis and other problems of the characteristics of the problem [23–26], and the rapidity of the feedforward control. An adaptive control strategy for flexible and fast braking of the free-fall hook system under a large inertia load is proposed. Our strategy can effectively reduce the pressure hysteresis loop and improve the pressure control accuracy, so as to improve the flexibility effect of the free-fall hook under the free-fall hook condition.

Meanwhile, in order to further match the output torque of the system with the load, different braking gears are divided for the loaded weight; the corresponding relationship between the pedal angle and the control current under different gears is established; and

different pedal control slopes are set up at different stages of system braking in order to expand the effective control stroke of the pedal and improve the resolution of the brake pedal. Finally, a simulation platform of the free-fall hook system built with MATLAB and AMESim software and the actual verification of the crawler crane free-fall hook system are used to prove the rationality and effectiveness of the strategy.

2. Modeling and Analysis of Free-Fall Hook Systems

2.1. Composition and Working Principle of Free-Fall Hook Systems

The principle of the free-fall hook system is shown in Figure 1, which mainly includes an electrical part, a hydraulic part, and a mechanical part. When the free-fall hook operation is performed, the input current of the pedal-controlled proportional pressure-reducing valve 2 decreases; the pressure in brake cavity 5 decreases; the pressure in cavity 6 remains stable and unchanged; the pressure difference between the two chambers of the clutch increases; the spring is compressed, causing the friction plate in the clutch to separate; and due to the effect of gravity, the load performs a free fall movement. When braking, the input current of the pedal-controlled proportional pressure-reducing valve 2 increases; the pressure in brake cavity 5 increases; the pressure difference between the two chambers of the clutch decreases; and the spring force causes the movable and static friction plates to come into contact and be pressed together, thus generating a braking torque and achieving free-fall hook braking.

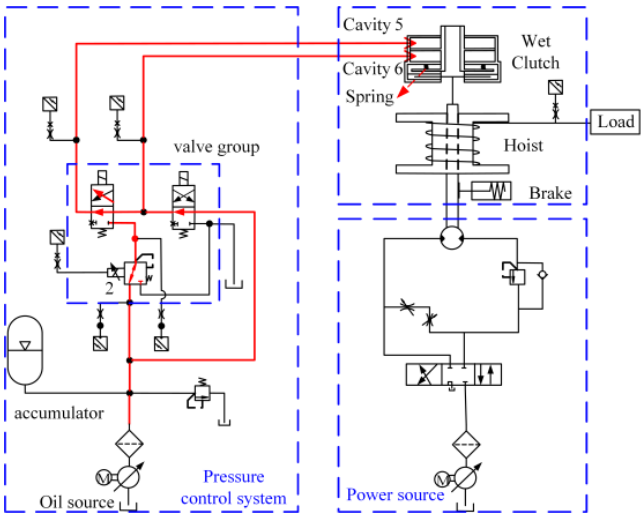

Figure 1. Schematic diagram of the free-fall hook system.

2.2. Mathematical Modeling and Characterization

2.2.1. Model of a Proportional Pressure-Reducing Valve

The proportional pressure-reducing valve is the core control element of the free-fall hook pressure control system. Its control signal can continuously and proportionally control the output pressure, which is approximately linear, and can realize high-precision conversion between electro-hydraulics.

1. Proportional Pressure-Reducing Valve Overflow Area Calculation

By disassembling and mapping the proportional pressure reducer, as shown in Figure 2, it can be determined that the effective displacement of the spool is 0.5 mm, and the maximum displacement of the spool is 1.6 mm. To calculate the micro-element area of the spool of the pressure-reducing valve under the valve opening x, the formula for calculating the spool overflow area is as follows.

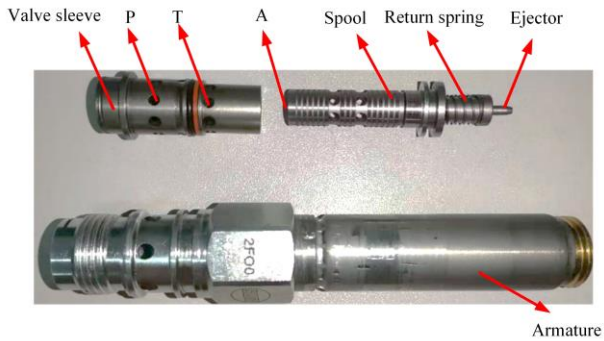

Figure 2. Pressure-reducing valve structure disassembly diagram.

When 1.1 < x < 1.6:

$$A = n \times \int_{1.1}^{x} \mathrm{d}A = n \times \left[R^2 \cdot \arccos \frac{R - x + 1.1}{R} - \sqrt{R^2 - (R - x + 1.1)^2} \cdot (R - x + 1.1) \right] \tag{1}$$

where A is the area of a single orifice, n is the number of orifices, and R is the diameter of the orifice of the pressure relief valve.

The change curve of spool overflow area with spool displacement is shown in Figure 3.

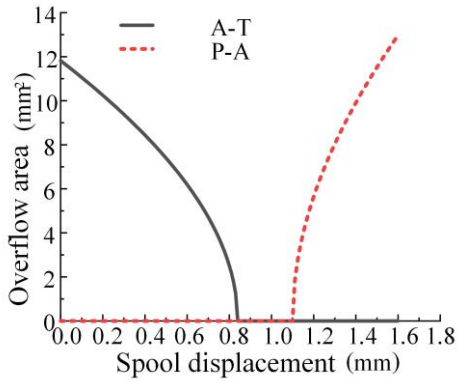

Figure 3. Valve port overflow area.

As can be seen in Figure 3, with the displacement of the spool, the A-T port overflow area gradually decreases. At the spool movement displacement of 0.84 mm, the A-T port is completely closed. At the displacement of 1.1 mm, the P-A port begins to open, and at the displacement of 1.6 mm, the P-A port overflow area is the largest and the P-A port is completely open. At this time, the proportional pressure-reducing valve outputs the maximum pressure.

2. Spool force analysis of proportional pressure-reducing valves

The equation for the output force of solenoid is:

$$F_{\mathrm{B}} = K_2 i + K_3 y \tag{2}$$

where i is the current value, K_2 is the electromagnet current–force gain coefficient, K_3 is the electromagnet displacement–force gain coefficient, and y is the armature displacement.

The equation for the spool force balance is:

$$F_{\mathrm{B}} - p_1 A_{\mathrm{v}} = K_{\mathrm{v}} x_{\mathrm{v}} + m_{\mathrm{v}} \frac{\mathrm{d}^2 x}{\mathrm{d}t^2} + (B_{\mathrm{s}} + B_{\mathrm{v}}) \frac{\mathrm{d}x}{\mathrm{d}t} + K_{\mathrm{f}} x_{\mathrm{v}} \tag{3}$$

where p_1 is the pressure-reducing valve orifice pressure, x_{v} is the pressure-reducing valve spool displacement, B_{s} is the transient hydrodynamic damping coefficient, K_{v} is the reset

spring stiffness of the pressure-reducing valve, A_v is the feedback area of the pressure-reducing valve, m_v is the mass of the pressure-reducing valve spool, B_v is the viscous damping coefficient of the spool, and K_f is the steady state hydrodynamic stiffness of the pressure-reducing valve.

2.2.2. Modeling of Free-Fall Hook Wet Clutches

In the first stage of the braking process (t_1–t_2), the dynamic and static friction plates are not in direct contact, the gap between the friction plates is filled with a film of oil, and there is only the phenomenon of band displacement torque. According to Newton's law of internal friction, the formula for calculating the slipping torque of a wet clutch is [27,28]:

$$T = n\frac{1}{2}\pi\eta W_{rel}({r_2}^4 - {r_1}^4)\sum_{i=1}^{n}\frac{1}{\delta_i} \tag{4}$$

where W_{rel} is the relative speed of the dynamic and static friction discs, n is number of contact surfaces on the dynamic and static friction discs, η is the dynamic viscosity of the lubricant, r_2 is the outer diameter of the friction disc, r_1 is the inner diameter of the friction disc, and δ_i is the dynamic and static friction disc gap.

In the free-fall hook system, brake cavity 5 is continuously supplied with oil, the pressure in brake cavity 5 increases, the pressure difference between brake cavity 5 and cavity 6 decreases, and the spring force overcomes the combined force between the two chambers, causing the piston to move. The equation for the instantaneous force balance of the piston is:

$$(p_s - p_0)A_P = k_p x_0 \tag{5}$$

where $A_p = \pi({r_2}^2 - {r_1}^2)$, p_s is the pressure in cavity 6, p_0 is the pressure in brake cavity 5, k_p is the stiffness coefficient of the reset spring, and x_0 is the initial compression of the reset spring.

From this, the pressure required in brake cavity 5 at t_1 of the first stage of braking is:

$$p_0(t_1) = p_s - \frac{k_p x_0}{A_p} \tag{6}$$

At the oil-filling stage (t_0–t_1), the flow rate of brake cavity 5 is $q(t_1)$, and the oil pressure in brake cavity 5 rises rapidly to $p_0(t_1)$, which pushes the piston to move to eliminate the gap between the movable and static friction discs. At this time, the pressure in the brake cavity 5 is expressed:

$$p_0 = p_s - \frac{k_p(x_0 - x_p) - m_p\ddot{x}_p - B_p\dot{x}_p}{A_p} \tag{7}$$

where x_p is the clutch piston displacement. Neglecting oil leakage, the flow balance equation is:

$$q = \frac{V_0}{\beta_e}\dot{p}_0 + A_p\dot{x}_p \tag{8}$$

where V_0 is the volume of brake cavity 5 and β_e is the volumetric modulus of elasticity of the fluid. Substituting Equation (6) into Equation (7) obtains:

$$q = \frac{V_0}{\beta_e A_p}\cdot(k_p\dot{x}_p + m_p\dddot{x}_p + B_p\ddot{x}_p) + A_p\dot{x}_p \tag{9}$$

Assuming that the piston moves at a constant speed in the first stage, the flow in brake cavity 5 is determined by the speed of piston movement and is a certain value.

$$q = (\frac{V_0}{\beta_e A_p}\cdot k_p + A_p)\dot{x}_p \tag{10}$$

To avoid flow fluctuations, let $q = q(t_1)$, then the time to eliminate the gap is Δt_{21}, and integrate over q:

$$p_0(t) = \frac{\beta_e k_p}{V_0 k_p + \beta_e A_p^2} q(t_1)(t - t_1) + p_0(t_1) \tag{11}$$

At the end of the first stage ($t = t_2$), the pressure in braking cavity 5 reaches:

$$p_0(t_2) = \frac{k_p h}{A_p} + p_0(t_1) \tag{12}$$

In the second stage of braking, also called the slippery wear stage (t_2–t_3), the movable and static friction plates come into contact and produce relative sliding. With the increase in pressure in brake cavity 5, the lubricant film between the movable and static friction plates is completely destroyed, in which the rough friction torque plays a major role, and the torque generated by this process makes the load brake. Ignoring the band-rolling torque, the torque calculation equation of friction vice [29,30] is:

$$T = n\mu R_m F_d \tag{13}$$

where u is the coefficient of kinetic friction of the friction disc and $R_m = \frac{2}{3}\frac{{r_0}^3 - {r_i}^3}{{r_0}^2 - {r_i}^2}$.

The acceleration of the load during braking is calculated as:

$$a = \frac{T \cdot i' - F_m R_d}{\sum m \cdot R_d} \tag{14}$$

where F_m is the tension on the wire rope, $\sum m$ is the total mass of the load, R_d is the radius of the winch, and i' is the transmission ratio between the winch and the output shaft of the clutch.

The pressure in brake cavity 5 at the completion of braking should reach $p_0(t_3)$:

$$p_0(t_3) = p_s - \frac{k_p(x_0 - x_{p_{max}})}{A_p} + \frac{T \cdot i'}{n\mu A_p} \tag{15}$$

In the third stage of braking, also called the full rough friction stage (t_3–t_4), the friction plate is affixed and pressed together, the movable and static friction plates are relatively static, and the torque generated by the clutch achieves full braking of the load. At this time, the friction type is static friction, and the torque calculation equation is:

$$T = n\mu_0 R_m F_d >> \sum F_m \cdot R \tag{16}$$

where μ_0 is the coefficient of static friction of the friction disc. The clutch brake cavity 5 pressure at this stage is:

$$p_0(t_4) > p_0(t_3) \tag{17}$$

2.2.3. Transfer Function of a Free-Fall Hook System

The first stage of clutch braking has little effect on braking, and this article focuses on the second and third stages of the braking process.

To model the second and third stages of clutch braking, the force equations for the spool of a proportional pressure-reducing valve are:

$$K_1 I - p_0 A_v = K_v x_v + m_v \frac{d^2 x}{dt^2} + (B_s + B_v)\frac{dx}{dt} + K_f x_v \tag{18}$$

The linear flow equation for a proportional pressure-reducing valve is:

$$q_L = K_q x_v - K_c p_0 \tag{19}$$

When the load flow rate is zero:

$$q = \frac{V_0}{\beta_e}\frac{dp_0}{dt} - C_{ip}(p_s - p_0) \tag{20}$$

carry out the Laplace transform:

$$\begin{cases} Q_L = K_q X_v - K_c P_0 \\ Q_L = \frac{V_0}{\beta_e} s P_0 + C_{ip} P_0 \\ K_1 I(s) - P_0 A_v = m_v s^2 X_v + (B_s + B_v) s X_v + (K_f + K_v) X_v \end{cases} \tag{21}$$

The resulting open-loop transfer function of the system is obtained as:

$$\frac{G(s)}{H(s)} = \frac{A_v K_q (\frac{V_0}{\beta_e} s + C_{ip} + K_c)^{-1}}{[m_v s^2 + (B_s + B_v)s + (K_f + K_v)]} \tag{22}$$

From the known parameters, the characteristic equation of the system is derived as:

$$1.7 \times 10^{-11} s^3 + 3.32 \times 10^{-8} s^2 + 1.2 \times 10^{-4} s + 0.15 = 0 \tag{23}$$

A stability analysis of the system is carried out. Based on the characteristic equations, a table of the Rouse criterion is presented as shown below:

$$\left| \begin{array}{l} s^3 1.7 \times 10^{-11} \; 1.2 \times 10^{-4} \\ s^2 3.32 \times 10^{-8} \; 0.15 \\ s^1 4.32 \times 10^{-5} \\ s^0 0.15 \end{array} \right. \tag{24}$$

According to Equation (24), the Rouse criterion table shows that the elements of the first column are all positive and the coefficients of the characteristic equations of the system are all positive, so the system is determined to be stable.

2.3. Nonlinear Characterization of a Free-Fall Hook System

2.3.1. Analysis of System Pressure Dead Band Characteristics

There is a dead zone in the free drop pressure control system. The dead zone of the system is mainly caused by the dead zone in the proportional pressure-reducing valve, which is an important factor affecting the performance of the proportional pressure-reducing valve [31]. The shoulder width of the valve core is usually slightly greater than the width of the valve mouth groove of the valve body when designing the two-position and three-way proportional pressure-reducing valve [32] so that the valve port overlap is formed, as shown in Figure 4 for the valve port schematic diagram. Due to the existence of the overlapping amount of the valve port, during the initial movement of the proportional pressure-reducing valve, the valve port will not have flow output, and clutch brake chamber 5 will not generate pressure. After the spool displacement is greater than the amount of covering, the valve port has a flow output, and clutch brake chamber 5 begins to build pressure. In the valve port covering stroke, the control signal cannot obtain the pressure response feedback of clutch brake chamber 5, and the overlapping part of the valve port causes the pressure dead zone, which is described by mathematical expression as:

$$q(x_v) = \begin{cases} 0 & x_v \le \Delta \\ Q(x_v) & x_v > \Delta \end{cases} \tag{25}$$

where $q(x_v)$ is the complete function of the flow rate with respect to the displacement of the spool, $Q(x_v)$ is a complete function of spool displacement, and x_v is the spool displacement.

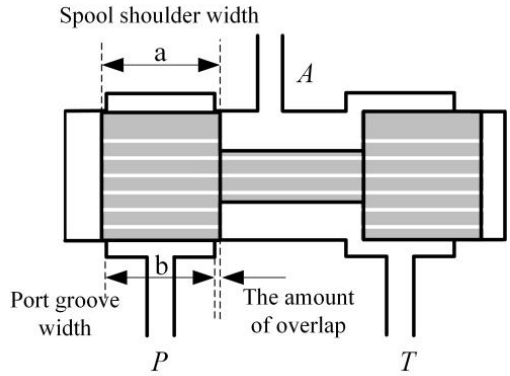

Figure 4. Schematic diagram of the valve port structure.

It is known that the coverage of the valve core of the proportional pressure-reducing valve is 1.1 mm, which is the dead zone of the valve core movement. It is determined that when the given current is less than 133 mA, the output pressure of the valve is zero, that is, the control current of the dead zone of the proportional pressure-reducing valve is 0–133 mA, as shown in Figure 5.

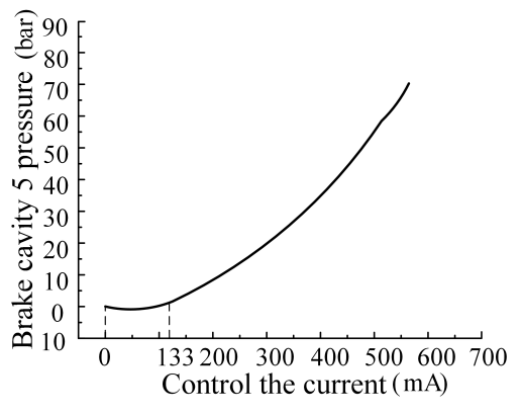

Figure 5. Current–pressure curve.

At the same time, according to the force analysis of the valve core, it can be seen that if the resultant force F is less than the static friction force of the valve core, the valve core is at rest, and the valve port of the proportional pressure-reducing valve will not have flow through, which is also one of the reasons for the dead zone. This article mainly considers the effect of the amount of valve port masking on the pressure of the system.

2.3.2. System Pressure Hysteresis

The presence of hysteresis in the system is mainly caused by proportional pressure-reducing valves, part of which is generated by the electromagnetic force output of the electromagnet, and the other part is generated by the movement of the valve core. According to the force balance equation of the valve core, under the same control current, when the valve core moves to the left and the right, the force of the valve core is different, resulting in the pressure hysteresis phenomenon of the valve core of the proportional pressure-reducing valve when it moves reciprocatingly. The main factors affecting the hysteresis of the spool of the proportional pressure-reducing valve are the transient hydraulic force, the steady-state hydraulic force, and the friction between the spool and the valve sleeve. Changes in the temperature of the system will cause changes in the viscosity of the oil, which will cause instantaneous changes in the hydraulic force, steady-state hydraulic force, and friction between the spool and sleeve, and increase the nonlinearity caused by the movement of the spool.

3. Research on the Control Strategy of the Free-Fall Hook System

Considering the non-linear characteristics of the free-fall hook system, such as dead zone and pressure hysteresis, this paper proposes to divide the free-fall hook brake gear according to the load weight and realize the automatic matching strategy of the load and brake gear, combined with the fuzzy PID controller, to achieve the optimal pressure control of the free-fall flexible on-load braking. The pressure control flow structure of the free-fall hook system based on automatic gear switching is shown in Figure 6.

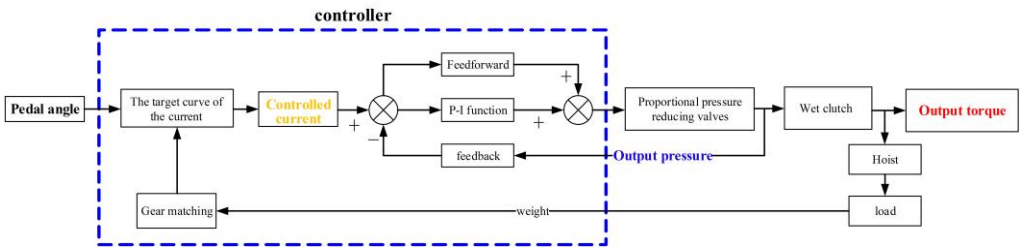

Figure 6. Flow chart of the control strategy.

3.1. Automatic Braking Gear Matching Control Strategy

Considering the different weights of the load, the free fall brake system is divided into different gears, and considering the recognition accuracy of the tension sensor, it is divided into five braking gears. The braking gears have different pedal and current relationships, so as to improve the control accuracy of each braking gear and the resolution of pedal control and increase the handling. The controller will determine the corresponding gear according to the tension of the wire rope and finally establish the automatic shift matching logic control relationship of the "load-sensor-controller-gear setting".

The relationship between pedal angle and current is shown in Figure 7. When braking, the control stroke of the pedal is from 35° to 17.5°, and the total stroke is 17.5° because the dead zone range of the proportional pressure-reducing valve is 0–133 mA. Thus, the distribution density of the current in front of pedal 4° (35°–31°) is larger, and the current starting value is 200 Ma. The torque in this range is small, and there is no braking effect, so the pedal idle stroke can be quickly crossed. When the pedal angle is 31°–19°, the braking is effective. At 19° of the pedal, the torque output of the clutch is enough to brake the load, and finally, 1.5° (19°–17.5°) increases the current density. Torque surplus is provided to ensure work safety.

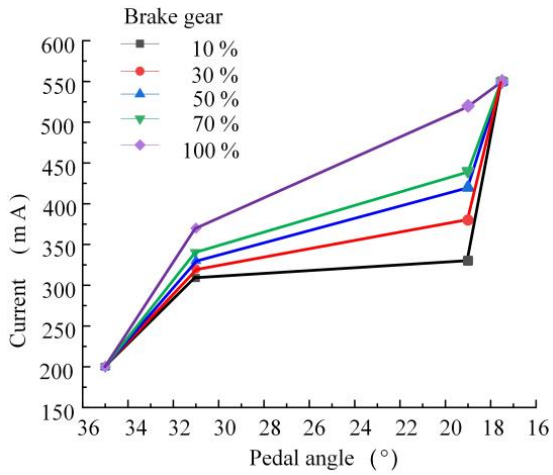

Figure 7. Correspondence between the pedal angle and control current.

3.2. Fuzzy Controller Design

A fuzzy PID controller [33], as shown in Figure 8, is used to accurately control the pressure in clutch brake cavity 5.

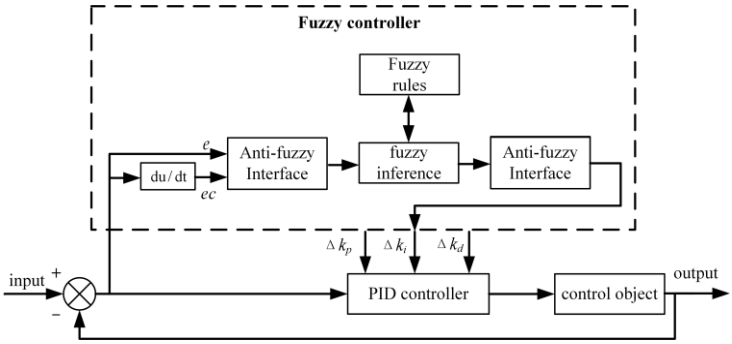

Figure 8. Fuzzy PID control schematic.

3.2.1. Define Inputs and Outputs

Using the test, a set of PID parameters to make the system relatively stable are preliminarily obtained, in which the scale coefficient k_{p0} = 0.05, the integration coefficient k_{p0} = 0.03, and the differential coefficient k_{p0} = 0.001.

The input of the fuzzy controller is the deviation between the target value of the pressure of brake cavity 5 and the actual value and the derivative of the deviation, and the output is the change in the three parameters of the PID controller, Δk_p, Δk_i, and Δk_d [34]. Taking the quantization domain of each variable of the controller as [−6, 6], and discretizing {−6, −5, −4, −3, −2, −1, 0, 1, 2, 3, 4, 5, 6} considering the complexity of the implementation and the control accuracy, this paper uses seven languages to design the fuzzy controller, and establishes that they are positive small (PS), positive medium (PM), positive large (PB), zero (Z), negative large (NB), negative medium (NM), and negative small (NS).

3.2.2. Determine the Affiliation Function

The role of the affiliation function is to convert the input into the corresponding fuzzy quantity. In order to meet the demand of free-fall hook control, we designed an Adaptive Precision Dynamic Fuzzy Controller (APD-FC) based on a hybrid affiliation function to balance the control accuracy in different error regions. The specific control idea is to use the triangular-shaped generosity function, which has high precision adjustment ability and high discrimination, in the small error region and the (NB) Z-shaped generosity function and (PS) the S-shaped generosity function, which can reduce the error quickly and have low discrimination, in the large error region [35,36]. The membership function curve is shown in Figure 9.

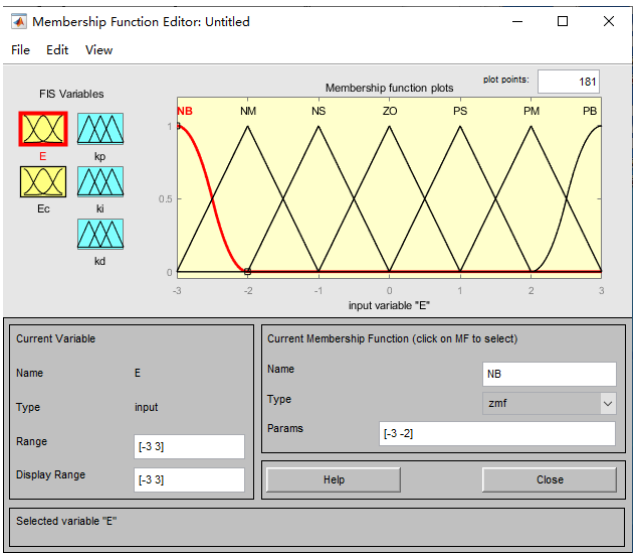

Figure 9. Membership function curve.

From Figure 9, the hybrid affiliation function used in this paper has the advantage of quickly reducing the current error and improving the accuracy of current control, thus improving the overall performance and efficiency of the control system.

3.2.3. Determining the Fuzzy Rules

According to actual engineering experience, the fuzzy rule relationship of PID parameter tuning is summarized as follows:

When the deviation e between the clutch brake cavity 5 pressure target value and the actual input value is very large, no matter how the derivative e_c of the deviation changes at this time, the proportional coefficient k_p should be increased so that the pressure error of the whole system is rapidly reduced. The coefficient k_i is usually set to zero to avoid integral saturation, and a smaller differential coefficient k_d is taken.

When the deviation e and the deviation conversion rate e_c of the pressure target value of clutch brake cavity 5 and the actual input value are positive or negative values at the same time, the absolute value of the pressure control error e of clutch brake cavity 5 increases. When the absolute value of e is large, a larger k_p should be used, and a smaller k_i and k_d should be used at the same time to improve the stability and dynamic performance of the system. When the absolute value of the error is smaller, a medium k_p value is used, and the k_i value is increased and the k_d value is reduced to improve the stability of the system.

When the positive and negative values of the error e and error conversion rate e_c are opposite, the absolute value of the pressure control error e of clutch brake cavity 5 decreases. When the absolute value of error e is smaller, a smaller k_p, a larger k_i, and a smaller k_d are used to improve the stability of the system and avoid system oscillation. When the absolute value of the deviation e is large, the stability of the system is improved by increasing the moderate k_p, the small k_i, and the moderate k_d [37–39].

3.2.4. Fuzzy Reasoning

The Mamdani inference method was chosen to determine the fuzzy output value. In the Mamdani method, when the conditional statement is "if E_i is A and E_{ci} is B then Δk_p is C", the expression calculated with the ith fuzzy rule R_i is:

$$R_i = (A \times B) \times C \tag{26}$$

According to the above equation, the values of fuzzy rules R_1 to R_{49} are found, respectively, and the total fuzzy rule R is obtained by calculating the total fuzzy rule, which is shown in Equation (27):

$$R = R_1 \cup R_2 \cup \cdots \cup R_{49} \tag{27}$$

The output values Δk_p, Δk_i, and Δk_d of the fuzzy control are calculated as shown in Equation (28):

$$\begin{cases} \Delta k_p = (E' \times E_c{}') \cdot R \\ \Delta k_i = (E' \times E_c{}') \cdot R \\ \Delta k_d = (E' \times E_c{}') \cdot R \end{cases} \tag{28}$$

3.2.5. Defuzzification to Obtain the Controller

According to Equation (29), to obtain the fuzzy control output value, the output value needs to be defuzzified to be recognized by the control object. This study uses the weighted average method for defuzzification and finally obtains a new PID parameter that contains the output of the fuzzy algorithm. The three PID parameter expressions are shown below:

$$\begin{cases} k_p = k_{p0} + \Delta k_p \\ k_i = k_{i0} + \Delta k_i \\ k_d = k_{d0} + \Delta k_d \end{cases} \tag{29}$$

Finally, based on the above analysis of fuzzy control principles and the control rules of the PID controller, the expression of the final controller u is determined, as shown in (30) [40]:

$$u = k_{\mathrm{p}} e(t) + k_{\mathrm{i}} \int_0^t e(t) \mathrm{d}\tau + k_{\mathrm{d}} \frac{\mathrm{d}e(t)}{\mathrm{d}t} \tag{30}$$

The transfer function of the PID controller is:

$$G_{\mathrm{c}}(\mathrm{s}) = K_1 + \frac{K_2}{\mathrm{s}} + K_3 \mathrm{s} \tag{31}$$

where $K_{\mathrm{p}} = K_1$, $\frac{K_{\mathrm{p}}}{T_{\mathrm{i}}} = K_2$, $K_{\mathrm{p}}\tau = K_3$.

The closed-loop transfer function is obtained after adding the PID controller:

$$\frac{G(s)}{H(s)} = \frac{\left(K_P + K_I \frac{1}{\mathrm{s}} + K_D s\right) \frac{A_v K_q \left(\frac{V_0}{\beta_e} s + C_{ip} + K_c\right)^{-1}}{[m_v s^2 + (B_s + B_v)s + (K_{\mathrm{f}} + K_v)]}}{1 + \left(K_P + K_I \frac{1}{\mathrm{s}} + K_D s\right) \frac{A_v K_q \left(\frac{V_0}{\beta_e} s + C_{ip} + K_c\right)^{-1}}{[m_v s^2 + (B_s + B_v)s + (K_{\mathrm{f}} + K_v)]}} \tag{32}$$

The closed-loop system characteristic equation is obtained as:

$$K_1 s^4 + K_2 s^3 + K_3 s^2 + K_4 s + K_5 = 0 \tag{33}$$

where $\begin{array}{l} K_1 = \frac{V_0}{\beta_e} m_v, K_2 = \left[\frac{V_0}{\beta_e}(B_s + B_v) + (C_{ip} + K_c) m_v\right], \\ K_3 = \left[\frac{V_0}{\beta_e}(K_{\mathrm{f}} + K_v) + (C_{ip} + K_c)(B_s + B_v) + K_D A_v K_q\right] \\ K_4 = \left[(C_{ip} + K_c)(K_{\mathrm{f}} + K_v) + K_P A_v K_q\right] \\ K_5 = K_I A_v K_q \end{array}$.

Since the coefficients of each term in the characteristic equation are all greater than 0, and the first column of elements in the Laws list obtained by substituting the parameters are all positive, the stability of the closed-loop system is proved.

4. Simulation Verification of the Control Strategy of the Free-Fall Hook System

AMESim and MATLAB Co-Simulation Platform

Using the powerful computational ability of MATLAB software, the flexible and fast braking control strategy of the free-fall hook system is built, and using the fidelity modeling characteristics of AMESim software, the simulation platform of a crawler crane free-fall hook system is built. With the use of interfaces, the joint simulation platform of free-fall hook high-performance adaptive control based on AMESim and MATLAB is obtained. The simulation model is shown in Figure 10.

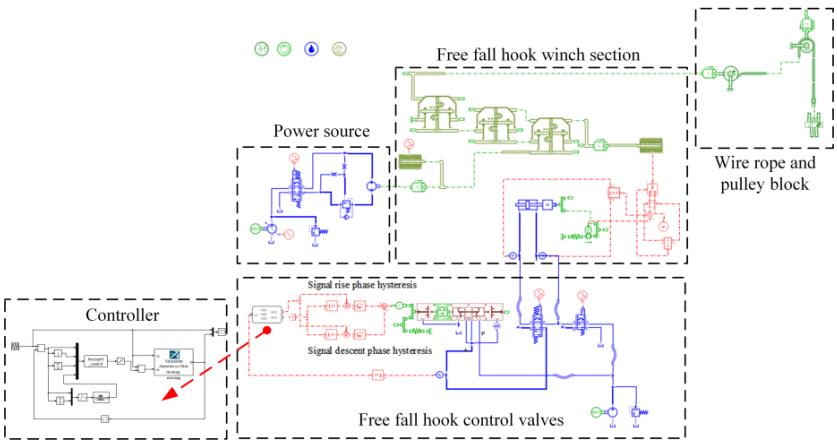

Figure 10. Simulation model of the free-fall hook system. Where: the red arrow points to the fuzzy controller simulation model.

The simulation parameters are shown in Table 1.

Table 1. Proportional pressure-reducing valve and wet clutch simulation parameters.

Simulation Parameters	Value
Spool mass, g	13.1
Return spring rate, N/mm	0.5
A, P spool diameter, mm	9.5
A, P inner cavity diameter, mm	8.7
The diameter of the inner lumen of the annular cavity, mm	9.5
The diameter of the spool of the annular cavity, mm	5.5
Spring preload. N	2.4
The outer diameter of the friction plate, mm	384
The inner diameter of the friction plate, mm	287
Spring rate, N/mm	3230
Spring preload, N	100,160
Piston stroke, mm	1.3
Piston diameter, mm	195
Piston rod diameter mm	125
Number of friction plate contact surfaces	15
Coefficient of static friction, mm	0.128

The hysteresis of the system was tested under different target pressures of brake cavity 5 and the improvement effect of the strategy on the hysteresis of the free hook pressure control system was verified. The height of the load from the ground was set to zero, the input signal of the proportional pressure-reducing valve was changed, the triangle wave excitation signal was set, the signal period was 10 s, and the amplitude was 70 bar, 60 bar, 50 bar, 40 bar, respectively. The hysteresis curve in Figure 11 is drawn according to the simulation data, and the hysteresis data of the statistical system is shown in Table 2.

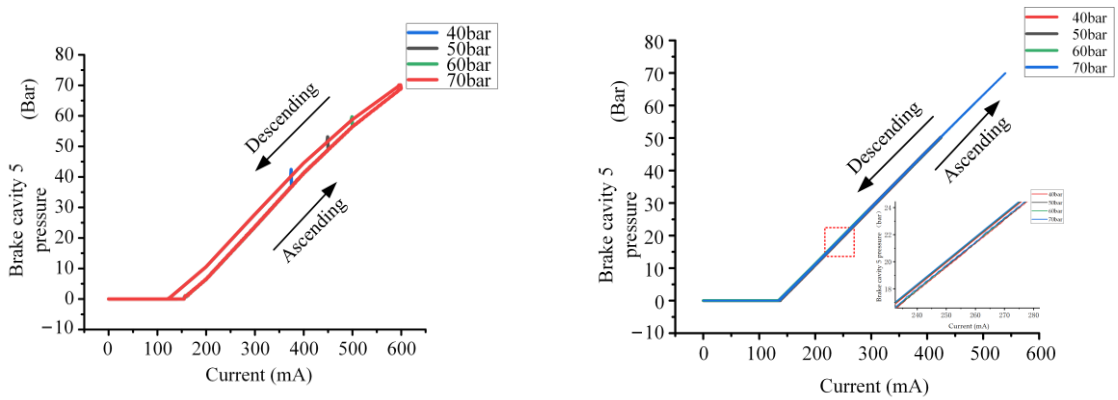

(**a**) (**b**)

Figure 11. Comparison of simulation effect before and after the control strategy: (**a**) the system hysteresis under different pressures before the strategy and (**b**) the system hysteresis at different pressures after the strategy.

Table 2. Hysteresis loop values before and after the control strategy.

Brake Cavity 5 Pressure (bar)	Hysteresis before the Strategy	Strategic Hysteresis Loop
40	8.86%	1.67%
50	8.11%	1.40%
60	9.56%	1.37%
70	9.82%	1.13%

In Figure 11, the pressure hysteresis loop curves show a consistent trend with commands of different amplitudes. After passing through the dead zone, the pressure increases and then decreases with the current change. Meanwhile, comparing Figure 11a,b, the pressure hysteresis loop phenomenon is significantly improved after optimization using the control strategy in this paper. According to Figure 11, the comparison data of pressure hysteresis before and after using the strategy under different instructions are shown in Table 2.

As can be seen from Table 2, under different command signals, the system hysteresis is more than 8% when the control strategy is not used. The system hysteresis is reduced to less than 2% and the system hysteresis is reduced by more than 75% after the control strategy is optimized so that the control strategy can effectively reduce the hysteresis of the system and improve the control accuracy of the pressure control system.

At the same time, in order to simulate the actual situation of the project, we consider a large load weight range of 6–10 tonnes, a hook weight of 0.44 tonnes, the use of 6.44 tonnes and 10.44 tonnes of two groups of loads, a height set to 4 m, and the use of the collected current signal during the test of the whole machine as the simulation model input signal, respectively. We use the experimental no-control strategy, the split-position strategy, and the split-position combined with the closed-loop pressure control under three conditions to determine the maximum acceleration of the system during braking. The results are shown in Figure 12.

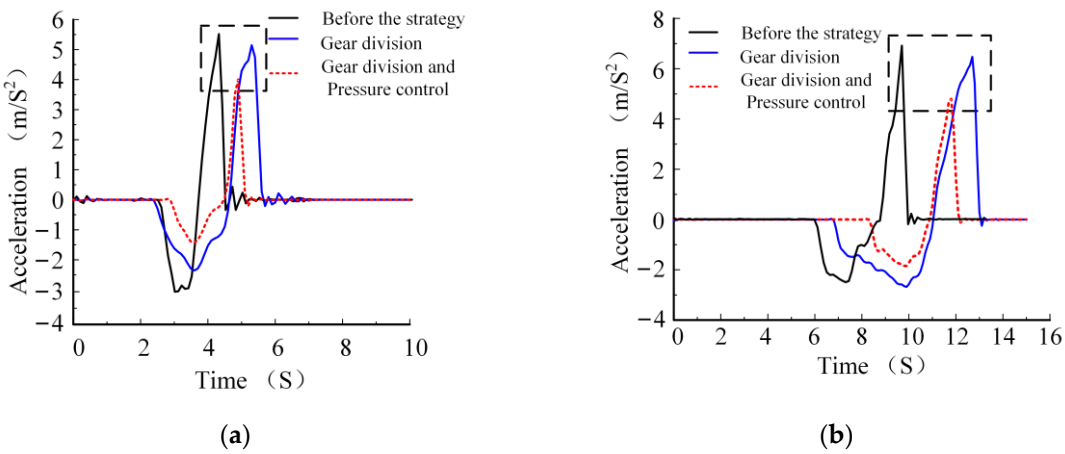

Figure 12. Comparison of braking acceleration for loads of 6.44 and 10.44 tonnes: (**a**) brake acceleration comparison for a load of 6.44 tonnes and (**b**) brake acceleration comparison for a load of 10.44 tonnes. Where: the black dashed box in the figure indicates the peak acceleration change that is the focus of this paper.

In Figure 12a,b, firstly, the acceleration increases from 0 m/s^2 to the maximum value along the negative direction of the Y-axis, which indicates that the load accelerates down. Secondly, the braking torque causes the acceleration to decrease, and when the braking torque is balanced with the load torque, the acceleration is 0 m/s^2. Finally, as the braking torque increases, the load starts to decelerate and brake, the braking acceleration increases along the positive direction of the Y-axis from 0 m/s^2 to reach the peak value, and then decreases to 0 m/s^2, and the load is braked. In this case, the peak braking acceleration is the largest before using the control strategy, decreases after using gear division, and is the smallest when using a combination of gear division and the pressure control strategy. Comparing Figure 12a,b, under the same conditions, the peak braking acceleration of the load of 10.44 tonnes is greater than the peak braking acceleration of the load of 6.44 tonnes. A comparison data of the braking effect before and after the use of the flexible braking control strategy under different loads is shown in Table 3.

Table 3. Comparison of peak braking acceleration before and after the strategy.

Load (t)	Strategy Front (m/s^2)	Gear Division (m/s^2)	Shift and Pressure Control (m/s^2)
6.44	5.56	5.15	4.02
10.44	6.77	6.47	4.80

According to the data in Table 3, under different loads, the braking acceleration before the control strategy is the largest. The maximum acceleration is reduced by simply using the gear division strategy, and the acceleration is minimized by using gear shift and pressure closed-loop control at the same time. Overall, the smaller the braking acceleration, the better the braking flexibility effect. At 6.44 tonnes, the maximum braking acceleration is reduced from 5.56 m/s^2 to 4.02 m/s^2, amounting to a decrease of 27.7%. At 10.44 tonnes, the maximum braking acceleration is reduced from 6.77 m/s^2 to 4.80 m/s^2, amounting to a decrease of 30.0%. The simulation results show that the shift combined with the pressure closed-loop control strategy can reduce the acceleration of load braking, which meets the flexibility requirements.

5. Experimental Study of the Flexible Control of the Free-Fall Hook System

5.1. Experimental Bench Study

Build the reducer clutch test setup as shown in Figure 13. Using the valve group of the free-fall hook system to control the pressure of braking chamber 5, the pressure of chamber 6 is controlled by the overflow protection effect of the relief valve, the free-fall hook action is simulated with the servomotor-driven rotation of the winch drum, and finally, the control effect of the pressure control strategy is verified. The core parameters of the proportional pressure-reducing valve and reducer clutch are consistent with those of the simulation model, and the experimental schematic diagram is shown in Figure 14.

(**a**) (**b**)

Figure 13. Installation diagram of the bench equipment: (**a**) horizontal test bench and (**b**) reducer clutch.

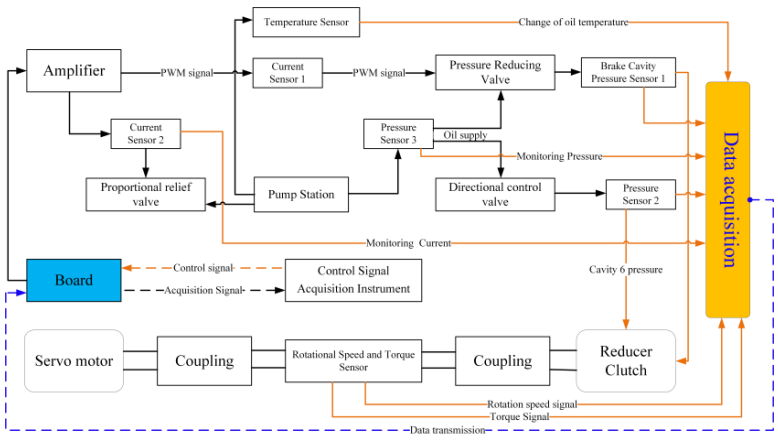

Figure 14. Schematic diagram of the bench test experiment.

During the test, the constant pressure value of chamber 6 is given, and the triangle wave control signal of different amplitudes of cavity 5 is given, as shown in Table 4.

Table 4. Command signal.

Brake Cavity 5 Pressure (bar)	Hysteresis before the Strategy	Strategic Hysteresis Loop
50	0-50-0	10
55	0-55-0	10
60	0-60-0	10
65	0-65-0	10
70	0-70-0	10
75	0-75-0	10
80	0-80-0	10
85	0-85-0	10
90	0-90-0	10

The pressure hysteresis curve of the free-fall hook system is plotted in Figure 15. The system hysteresis for each condition was calculated according to the hysteresis formula, and the statistics are shown in Table 5.

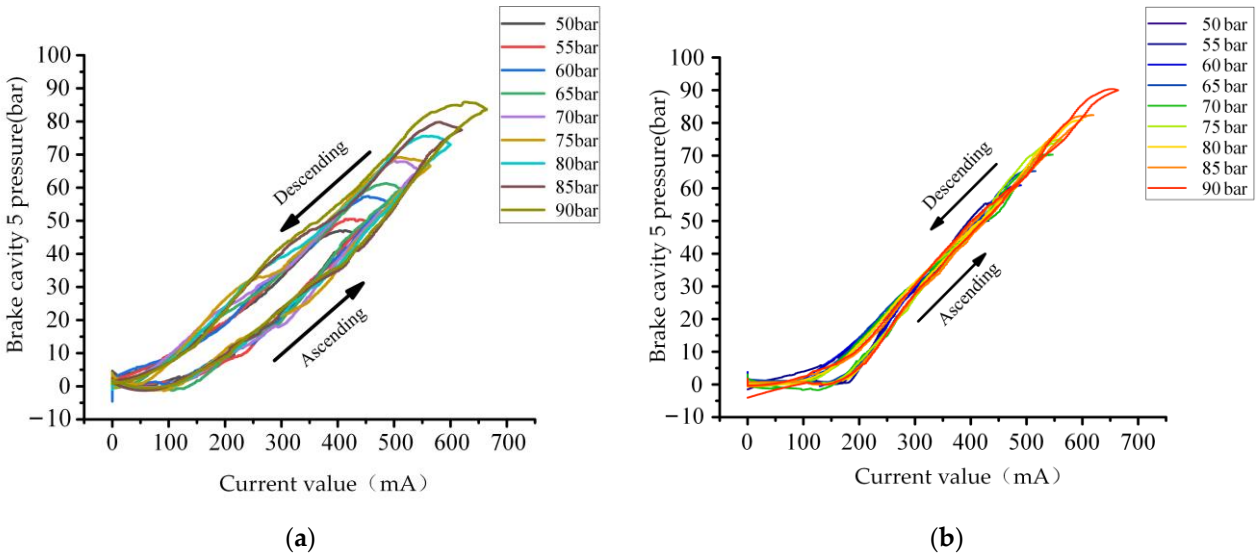

(**a**) (**b**)

Figure 15. Pressure hysteresis loop of the free-fall hook system bench test: (**a**) hysteresis before the strategy and (**b**) post-strategy hysteresis loop.

Table 5. System hysteresis loop at different brake chamber pressures.

Brake Cavity 5 Pressure (bar)	Hysteresis before the Strategy	Strategic Hysteresis Loop
50	18.53%	6.93%
55	17.43%	2.27%
60	17.39%	1.40%
65	16.13%	3.21%
70	16.02%	1.73%
75	16.00%	2.22%
80	15.38%	3.31%
85	16.09%	2.81%
90	14.75%	1.37%

Comparing Figure 15a,b, the pressure hysteresis loop is significantly reduced after optimization using the control strategy, which further validates the effectiveness of the strategy. The actual physical system has uncertainties such as friction [41], resulting in

the deviation om the experimental results from the simulation hysteresis loop simulation. However, based on the control strategy in this paper, both have better control effects. According to Figure 15, a comparison data of the actual test pressure hysteresis loop control effect before and after the use of the control strategy under different instructions is shown in Table 5.

Based on the bench test of the free-fall hook system, the hysteresis loop is 14%–19% before the control optimization, and after the control strategy optimization, the hysteresis loop is larger when the pressure in the brake chamber is 50 bar and the hysteresis loop is 6.93%, and the hysteresis loop of the system is stable at 2%–3% in other cases. The hysteresis loop of the system is reduced by more than 80%, and the linearity of the pressure control of the free fall hook system is improved.

5.2. Analysis of the Free-Fall Hook Process

Taking the load of 10.44 tonnes as an example, the system signal control flow and free-fall hook action analysis were completed, as shown in Figure 16.

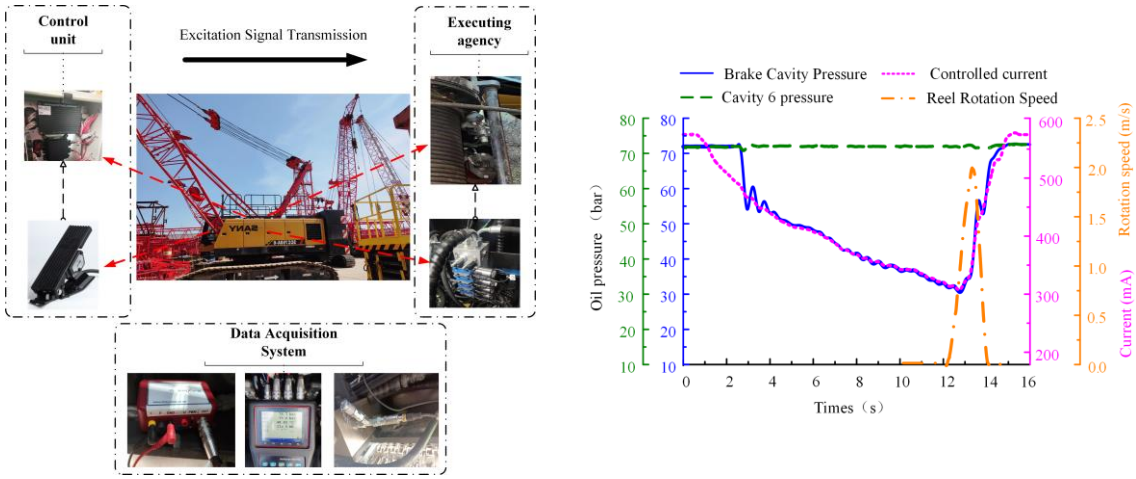

(**a**) (**b**)

Figure 16. Free-fall hook condition field test and process analysis: (**a**) system control signal flow chart and (**b**) free-fall hook action for a load of 10.44 tonnes.

The free-fall hook system controller output current is controlled by the electric pedal angle, which in turn acts on the electric proportional pressure-reducing valve to control the pressure after the valve and ultimately controls the torque output of the clutch. Data acquisition includes pedal angle, proportional valve control current, post-valve pressure, reel speed, and so on.

As can be seen from (b), the clutch cavity pressure is basically stable at about 72 bar, the control current of the free-fall hook system and the brake cavity pressure change synchronously. When the free-fall hook system opening button is pressed at 1.0 s, the brake cavity pressure starts to be controlled by the proportional pressure-reducing valve, the current signal of the proportional valve starts to decrease from about 550 mA at 2.5 s, and the brake cavity pressure decreases with the same trend, but there is an obvious delay in comparison with the current change trend. The brake chamber pressure decreases with the same trend, but there is an obvious delay compared with the current trend. When the brake chamber pressure decreases to 32 bar in 12 s, the drum starts to move, the rotating speed gradually increases from zero, and the weight starts to fall. When the pressure in the braking chamber increases to 40 bar with the proportional pressure-reducing valve control current, the reel speed starts to decrease. When the pressure in the clutch braking chamber increases to about 60 bar in 14 s, the reel speed decreases to 0, and the braking process and the free-fall hook action ends.

5.3. Analysis of the Hysteresis Loop and Braking Acceleration

In order to further verify the effectiveness of the control strategy proposed in this paper, the system pressure hysteresis loop and braking acceleration are tested under different weights of loads, respectively, as shown in Figure 17. The data comparison of the control effect is shown in Table 6.

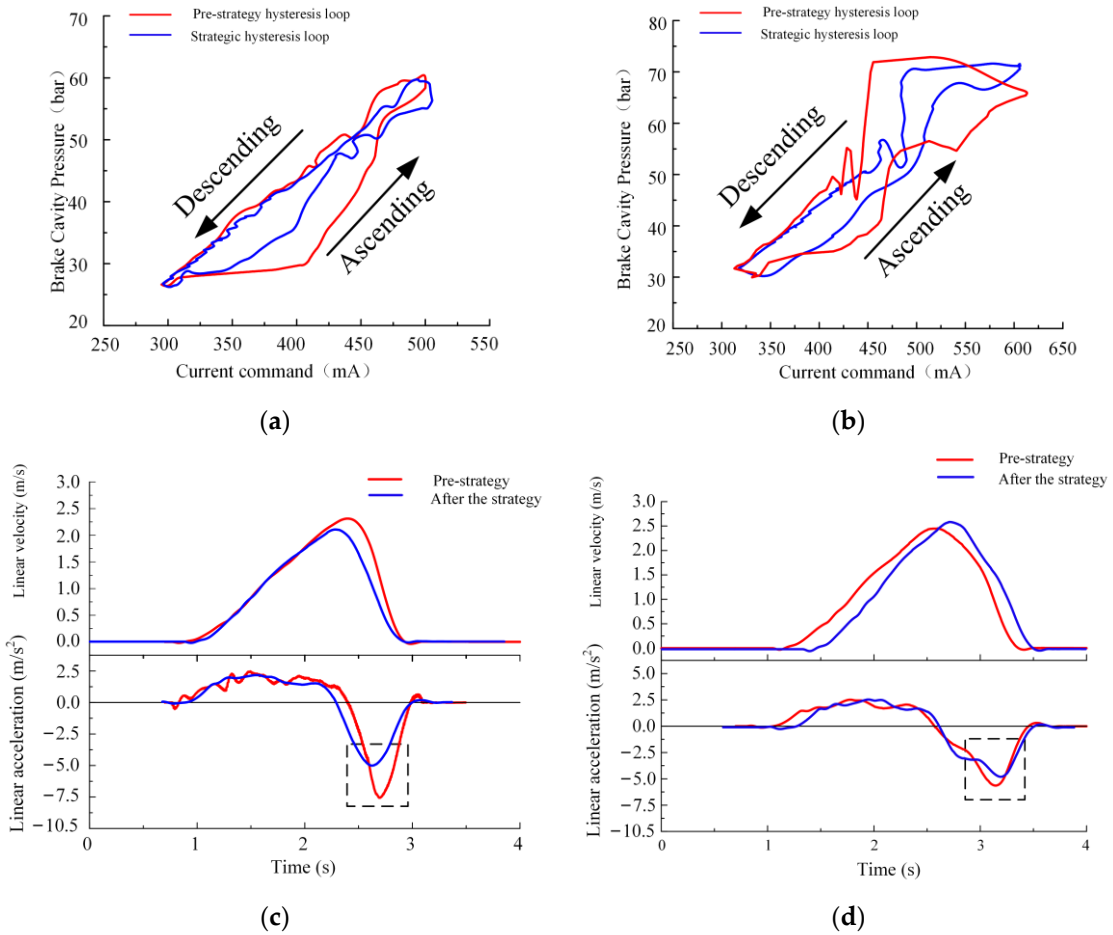

Figure 17. Comparison of system pressure hysteresis loop and braking acceleration before and after the control strategy: (**a**) system pressure hysteresis at a load of 6.44 tonnes; (**b**) system pressure hysteresis at a load of 10.44 tonnes; (**c**) braking acceleration at a load of 6.44 tonnes; and (**d**) braking acceleration at a load of 10.44 tonnes. Where: the black dashed box in the figure indicates the peak acceleration change that is the focus of this paper.

Table 6. Hysteresis loops and acceleration variations.

Load (t)	Strategy Front		After the Strategy	
	Hysteresis Loop	Acceleration (m/s^2)	Hysteresis Loop	Acceleration (m/s^2)
6.44	24.75%	7.56	11.87%	5.20
10.44	25.82%	6.217	10.21%	4.71

In Figure 17a,b, the pressure hysteresis phenomenon is significantly reduced after using the control strategy under the different loads. The results of the whole-vehicle experiments are consistent with those of the simulation experiments and the bench experiments, which further verifies the practicability of the control strategy in this paper. At the same time, these results further illustrate that the fuzzy PID control method is capable of effectively compensating for the pressure variations [26].

In Figure 17c,d, it can be seen that a positive value of acceleration indicates that the load is accelerating down and a negative value indicates decelerating braking. Both groups of experiments show that the peak braking acceleration before the strategy is significantly larger than that after the strategy, which indicates that the control strategy effectively reduces the peak braking acceleration, thus proving the effectiveness of the strategy. Under different loads, a comparison of the data for the experimental braking effect of the whole vehicle before and after the use of the flexible braking control strategy are shown in Table 6.

Table 6 shows that the system pressure hysteresis loop decreases from 24.75% to 11.87% with a load of 6.44 tonnes, amounting to a decrease of 52.04%, and from 25.82% to 10.21% with a load of 10.44 tonnes, amounting to a decrease of 60.45%. In the literature [42] on proportional pressure-reducing valves, the hysteresis loop is only reduced by 50% using the interval constant value compensation control scheme, while the system hysteresis loop is reduced by more than 50% using the control strategy proposed in this paper. This proves the effectiveness of the strategy in this paper.

At a load of 6.44 tonnes, the maximum acceleration under braking decreases from 7.56 m/s^2 to 5.20 m/s^2, amounting to a decrease of 31.22%. The maximum acceleration under braking decreased from 6.217 m/s^2 to 4.71 m/s^2 with a load of 10.44 tonnes, amounting to a decrease of 24.24%.

The results show that the closed-loop control strategy of shift combination pressure has obvious improvement effects. The clutch torque output accuracy is also improved, the clutch pressure control accuracy is improved [43], and the smoothness during braking is obviously improved. The experimental results of the whole machine are similar to those of the simulation experiments, which proves the accuracy of the simulation model.

6. Limitations and Future Work

We consider the following as limitations of the experimental conditions: first, the experimental objects are two groups of loads of 6.44 tonnes and 10.44 tonnes, with limited sample capacity. In the future, in order to further verify the effectiveness of the control strategy in this paper, we will increase the experimental sample capacity and conduct more comparative experiments using other affiliation functions and control methods. Second, the simulation experiments conducted in MATLAB and AMESim software cover the typical working conditions of a free-fall hook, such as flexible lowering with load, free-fall hook with load braking, point brake braking, SDDC conditions, etc., but they do not include all the functions of the free-fall hook system, such as the power priority and the heavy load cycling, etc. In addition, there are assumptions and simplification limitations of some of the components in the model established, such as the pulley block and the wire rope. In the future, the simulation model will be calibrated using experimental data to ensure that it reflects the state of the actual system, and secondly, deficiencies in the simulation model will be identified and corrected by comparing the simulation results with experimental or actual data.

7. Conclusions

In this paper, the nested control method is used to solve the problem that the braking of the free-falling hook condition of large tonnage crawler cranes is prone to impact, and flexible and smooth braking control is realized. Among them, the pressure output characteristics of the proportional pressure-reducing valve are clarified, and the flexible braking control strategy of the free-falling hook system is proposed. The specific conclusions are as follows:

(1) For the free-falling hook system with large inertia and strong impact characteristics, the dead zone and hysteresis loop characteristics of the proportional decompression valve pressure output are obtained, and the control strategy of dividing the braking gears, assigning different current slopes at different stages, and automatically matching the mechanism of load weight, combined with the feed-forward and fuzzy PID pressure closed-loop, is proposed.

(2) Based on the nested closed-loop control strategy in this paper, the system hysteresis loop is only 11%, which is more than 50% lower than before.
(3) After using the control strategy, the maximum braking acceleration is reduced by 31.22% for a load of 6.44 tonnes and by 24.24% for a load of 10.44 tonnes, which significantly improves the flexible and smooth braking effect of a free-fall hook with a load.

The research in this paper provides a theoretical basis and reference for the research of free-fall hook flexible braking for large tonnage crawler cranes, which helps the intelligent transformation of crawler cranes.

Author Contributions: Conceptualization, W.G., S.S. and W.X.; methodology, L.C.; software, Y.W.; validation, G.Y. and W.X.; formal analysis, Y.W.; investigation, W.G.; resources, C.W. and C.A.; data curation, G.Y. and W.X.; writing—original draft preparation, S.S.; writing—review and editing, S.S.; supervision, L.C.; project administration, C.A. and W.G.; funding acquisition, C.A. All authors have read and agreed to the published version of the manuscript.

Funding: This research was funded by the National Natural Science Foundation of China, grant number 52205060, the Hebei Natural Science Foundation, grant number E2021203020 and the Postgraduate Research & Practice Innovation Program of Jiangsu Province, grant number SJCX22_1043.

Data Availability Statement: Data are contained within the article.

Conflicts of Interest: Author Chunyi Wang was employed by the company Zhejiang Sany Equipment Company Limited. The remaining authors declare that the research was conducted in the absence of any commercial or financial relationships that could be construed as a potential conflict of interest.

References

1. Shaikh, A. Lifting capacity enhancement of a crawler crane by improving stability. *J. Theor. Appl. Mech.* **2016**, *54*, 219–227. [CrossRef]
2. Tuan, L.A.; Lee, S.-G. Modeling and advanced sliding mode controls of crawler cranes considering wire rope elasticity and complicated operations. *Mech. Syst. Signal Process.* **2018**, *103*, 250–263. [CrossRef]
3. Muhammad, A.G.; Asif, M.; Shuai, L.; Jacek, O.; Ahmed, B.; Mohamed, A.-H. Decision support for hydraulic crane stabilization using combined loading and crane mat strength analysis. *Autom. Constr.* **2021**, *131*, 103884.
4. Hao, H.; Ma, H. Optimizing Gearshift Control of Wet Dual Clutch Transmission. *Mech. Sci. Technol. Aerosp. Eng.* **2022**, *41*, 936–947.
5. Yan, H.; Xu, S.; Tan, W.; Wu, J.; Zhang, Y. Study on dynamic engagement characteristics of friction clutch under input fluctuating speed. *Mod. Manuf. Eng.* **2021**, *10*, 33–39.
6. Wu, B.; Qin, D.; Hu, J.; Wang, X.; Wang, Y.; Lv, H. Analysis of influencing factors and changing laws on friction behavior of wet clutch. *Tribol. Int.* **2021**, *162*, 107125. [CrossRef]
7. Wang, C.; Qin, D.T.; Wu, B.Z.; Fang, H.S.; Cheng, K. Simulation and analysis of wet clutch engagement characteristics. *J. Chong-Qing Univ.* **2020**, *43*, 38–51.
8. Heng, Z.; Heyan, L. Experimental Study on Attenuation Characteristics of Friction Torque Transferred by the Wet Multi-disc Clutch. *J. Harbin Inst. Technol.* **2018**, *50*, 94–102.
9. Yang, C.; Wu, P.; Shang, X.; Wang, Z. Simulation and experimental study of engagement process with groove consideration. *J. Zhejiang Univ. Eng. Sci.* **2019**, *53*, 1225–1236.
10. Meng, Q.; Tian, Z.; Zhao, C. Non-uniform contact characteristics of the friction disc during the initial period of a braking process. *J. Mech. Sci. Technol.* **2018**, *32*, 1261–1268.
11. Fei, J.; Luo, W.; Huang, J.F.; Ouyang, H.; Xu, Z.; Yao, C. Effect of carbon fiber content on the friction and wear performance of paper-based friction materials. *Tribol. Int.* **2015**, *87*, 91–97. [CrossRef]
12. Yu, L.; Ma, B.; Chen, M.; Li, H.; Ma, C.; Liu, J. Comparison of the Friction and Wear Characteristics between Copper and Paper Based Friction Materials. *Materials* **2019**, *12*, 2988. [CrossRef] [PubMed]
13. Liu, Y.; Chen, M.; Yu, L.; Wang, L.; Feng, Y. Influence of Material Parameters on the Contact Pressure Characteristics of a Multi-Disc Clutch. *Materials* **2021**, *14*, 6391. [CrossRef] [PubMed]
14. Padmanabhan, S.; Vinod Kumar, T.; Sendil Kumar, D.; Velmurugan, G.; Akshay Kumar, B.; Hitesh Sri Subramanyam, K. Investigation of structural and thermal analysis of clutch facings with different friction materials. *Mater. Today Proc.* **2023**, *92*, 98–105. [CrossRef]
15. Bao, H.Y.; Xu, T.J.; Jin, G.H.; Huang, W. Analysis of Dynamic Engaged Characteristics of Wet Clutch in Variable Speed Transmission of a Helicopter. *Processes* **2020**, *8*, 1474. [CrossRef]
16. Lu, K.; Wang, L.; Lu, Z.; Zhou, H.; Qian, J.; Zhao, Y. Sliding Mode Control for HMCVT Shifting Clutch Pressure Tracking Based on Expanded Observer. *Trans. Chin. Soc. Agric. Mach.* **2023**, *54*, 410–418.

17. Kuang, J.K. Control of electro-hydraulic actuated clutch system based on nonlinear feed-forward controller. *China J. Constr. Mach.* **2022**, *20*, 199–204.
18. Fu, S.; Gu, J.; Li, Z.; Mao, E.; Du, Y.; Zhu, Z. Pressure Control Method of Wet Clutch for PST of High-power Tractor Based on MFAPC Algorithm. *Trans. Chin. Soc. Agric. Mach.* **2020**, *51*, 367–376.
19. Zhang, C.; Yu, H.; Shi, W.; Liu, Q.; Hong, J.; Gao, B. Nonlinear Pressure Control of Electronically Controlled Hydraulic Direct Drive Multi-Disc Clutch. *Trans. Beijing Inst. Technol.* **2022**, *42*, 850–856.
20. Qin, Y.; Gong, G.; Wang, F.; Sun, C. Research on pressure control strategy of hydraulic system of hydro-viscous variable speed clutch. *J. Harbin Eng. Univ.* **2020**, *41*, 1377–1383.
21. Zhang, Y.A.; Du, Y.F.; Meng, Q.F.; Li, X.Y.; Liu, L.; Zhu, Z.X. Model-free adaptive control of tractor wet clutch pressure based on improved ge-netic algorithm. *J. Jilin Univ. (Eng. Ed.)* **2023**, 1–14. [CrossRef]
22. Zhang, Y.A.; Du, Y.; Mao, E.; Song, Z.; Chen, D.; Zhu, Z. Pressure Control Method of Wet Clutch in High-powered Tractor Based on Digital Twin. *J. Mech. Eng.* **2023**, *59*, 268–279.
23. Yu, Z.; Dong, H.M.; Liu, C.M. Research on Swing Model and Fuzzy Anti Swing Control Technology of Bridge Crane. *Machines* **2023**, *11*, 579. [CrossRef]
24. Hasan, M.W.; Mohammed, A.S.; Noaman, S.F. An adaptive neuro-fuzzy with nonlinear PID controller design for electric vehicles. *IFAC J. Syst. Control* **2024**, *27*, 100238. [CrossRef]
25. Huang, X.; Lu, Z.; Chen, L.; An, Y. Research on Fuzzy PID Control of HMCVT Pump-Controlled-Motor System. *Acta Agric. Univ. Jiangxiensis* **2023**, *45*, 189–201.
26. Li, A.; Qin, D.; Guo, Z.; Xia, Y.; Lv, C. Wet clutch pressure hysteresis compensation control under variable oil temperatures for electro-hydraulic actuators. *Control Eng. Pract.* **2023**, *141*, 105723. [CrossRef]
27. Zhang, L.; Wei, C.; Hu, J. Optimization design of low drag torque parameters of high- speed multi- plate wet clutch. *Automot. Eng.* **2020**, *42*, 1074.
28. Li, J.; Ma, C.; Wang, X. Research on Drag Torque Characteristics of Wet Clutchs under High Linear Speed Conditions. *China Mech. Eng.* **2023**, *34*, 2693.
29. Cheng, X.; Zhu, M.; Tian, N. Numerical analysis of effect of liquid-gas two-phase flow on the drag torque characteristics of wet clutch. *Acta Armamentarii* **2020**, *41*, 850.
30. Rogkas, N.; Vasilopoulos, L.; Spitas, V. A hybrid transient/quasi-static model for wet clutch engagement. *Int. J. Mech. Sci.* **2023**, *256*, 108507. [CrossRef]
31. Li, C.; Lyu, L.T.; Helian, B.B.; Chen, Z.; Yao, B. Precision Motion Control of an Independent Metering Hydraulic System with Nonlinear Flow Modeling and Compensation. *IEEE Trans. Ind. Electron.* **2022**, *69*, 7088–7098. [CrossRef]
32. Wang, T.; Song, Y.; Huang, L.S.; Fan, W. Parameter Tuning Method for Dither Compensation of a Pneumatic Proportional Valve with Friction. *Chin. J. Mech. Eng.* **2016**, *29*, 607–614. [CrossRef]
33. He, J.; Su, S.; Wang, H.; Chen, F.; Yin, B. Online PID Tuning Strategy for Hydraulic Servo Control Systems via SAC-Based Deep Reinforcement Learning. *Machines* **2023**, *11*, 593. [CrossRef]
34. Guo, Q.; Han, J.; Peng, W. PMSM Servo Control System Design Based on Fuzzy PID. In Proceedings of the 2nd International Conference on Cybernetics, Robotics and Control (CRC), Chengdu, China, 21–23 July 2017; pp. 85–88.
35. Varshney, A.; Goyal, V. Re-evaluation on fuzzy logic controlled system by optimizing the membership functions. *Mater. Today Proc.* **2023**. [CrossRef]
36. Lu, W.; Guo, K.; Zhang, J. Feed-forward integrated with fuzzy PID feedback current control algorithm in electric power steering. *Trans. CSAM* **2010**, *41*, 10–15.
37. Mao, H.Y.; Si, Y.N.; Fan, J.W.; Li, X.P. Research of Fuzzy PID Controller Implemention Method Based on PLC. In Proceedings of the Seventh International Conference on Measuring Technology and Mechatronics Automation (ICMTMA 2015), Nanchang, China, 13–14 June 2015; pp. 823–826.
38. Petrov, M.; Ganchev, I.; Taneva, A. Fuzzy PID control of nonlinear plants. In Proceedings of the 1st International IEEE Symposium on Intelligent Systems, Varna, Bulgaria, 10–12 September 2002; pp. 30–35.
39. Ge, X.; Du, C. Tuning of fuzzy internal mode PID control parameters for first-order time delay system. *Exp. Technol. Manag.* **2023**, *40*, 104–108.
40. Chen, K.; Zhou, H.; Shan, X. Rotation-control device for construction cranes with nested PID control. *Autom. Constr.* **2023**, *146*, 104704. [CrossRef]
41. Jung, S.; Choi, S.B.; Ko, Y.; Kim, J.; Lee, H. Pressure control of an electro-hydraulic actuated clutch via novel hysteresis model. *Control Eng. Pract.* **2019**, *91*, 104112. [CrossRef]
42. Li, Z.; Chen, J.X.; Shi, X.X.; Ouyang, W.Q.; Ai, C. Study on hysteresis ring compensation of electro-hydraulic proportional pressure reducing valve. *Constr. Mach.* **2022**, *10*, 37–44+4.
43. Wu, J.; Cui, J.; Shu, W.; Wang, L.; Li, H. Coupling mechanism and data-driven approaches for high power wet clutch torque modeling and analysis. *Tribol. Int.* **2024**, *191*, 109166. [CrossRef]

Disclaimer/Publisher's Note: The statements, opinions and data contained in all publications are solely those of the individual author(s) and contributor(s) and not of MDPI and/or the editor(s). MDPI and/or the editor(s) disclaim responsibility for any injury to people or property resulting from any ideas, methods, instructions or products referred to in the content.